Chemical routes to materials

Oxidative degradation of sulfamethoxazole antibiotic catalyzed by porous magnetic manganese ferrite nanoparticles: mechanism and by-products identification

Yulian Li[1,2], Junyong He[1], Kaisheng Zhang[1], Peidong Hong[1,2], Chengming Wang[3], Lingtao Kong[1,*] , and Jinhuai Liu[1]

[1] *Nano-Materials and Environmental Detection Laboratory, Institute of Intelligent Machines, Chinese Academy of Sciences, Hefei 230031, People's Republic of China*

[2] *Department of Chemistry, University of Science and Technology of China, Hefei 230026, Anhui, People's Republic of China*

[3] *Hefei National Laboratory for Physical Sciences At the Microscale, University of Science and Technology of China, Hefei 230026, Anhui, People's Republic of China*

ABSTRACT

Magnetic porous manganese ferrite nanoparticles ($Mn_xFe_{3-x}O_4$) with diverse ingredient Mn/Fe mole ratios were synthesized to degrade sulfamethoxazole (SMX) antibiotic residues involving peroxymonosulfate (PMS) dissociation to produce free radical $SO_4^{•-}$, $^•OH$ and singlet oxygen $^1O_2$ in the absence of heat and light. With the increase in proportion of manganese, the degradation efficiency of SMX increased from 19 to 70% in 30 min. The removal efficiency of SMX increased following the concentration increase of PMS (from 1 ~ 10 mM). After 60 min, the total organic carbon went down by 20%, and the concentration of NH_4^+ and NO_3^- accumulated obviously simultaneously. EPR study and chemical probe method, depending on scavenging revealed that $SO_4^{•-}$, $^•OH$ and $^1O_2$ were generated and contributed to the degradation system. Based on the capture of eleven decomposition by-products by LC/MS, two different degradation pathways of SMX were determined, mainly consisting of cleavage of the S–N bond, hydroxylation of benzene and heterocyclic ring, oxidation of amino group and ring-opening cleavage processes. The nanoparticle reuse tests showed that the porous magnetic manganese ferrite nanoparticles could still maintain a high degradation efficiency after five oxidative degradation reactions. The magnetic porous manganese ferrite nanocrystals could activate the PMS to oxidize SMX antibiotic residue without additional energy.

Address correspondence to E-mail: ltkong@iim.ac.cn

 Springer

GRAPHIC ABSTRACT
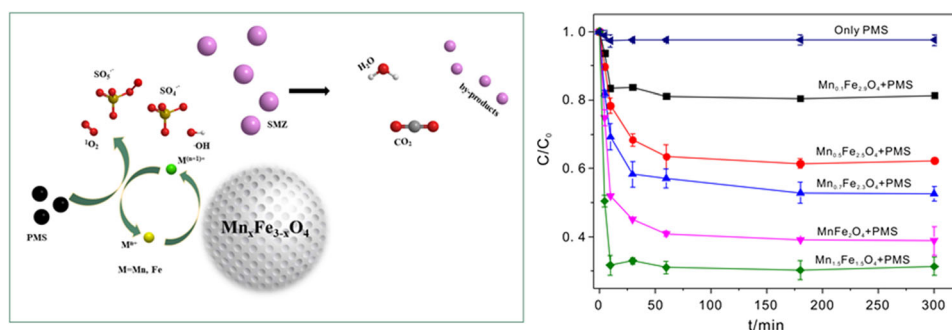
Introduction

Antibiotic environmental residues accelerate the development and spread of bacterial resistance and have become a global environmental health problem [1, 2]. They are mercilessly discharged into rivers and lakes by human beings and further into surface water, which brings about that the quality of water needed in daily life cannot be effectively guaranteed [3, 4]. It has been reported that various types of antibiotics, such as sulfonamides, β-lactamides, macrolides and quinolones, have been detected in the effluent of urban sewage treatment plants [5]. The world health organization (WHO) has identified bacterial resistance as the most serious problem facing humanity in the twenty-first century and proposed a global action plan to control antibiotic resistance in 2015 [5, 6]. Besides, sulfamethoxazole (N1-(5-methylisoxazol-3-yl)-4-aminobenzene-1-sulfonamide, SMX) is a frequently used sulfonamide antibiotic, mainly used for urinary tract infection, respiratory system infection, intestinal infection, biliary tract infection and local soft tissue or wound infection caused by sensitive bacteria. Drug abuse for humans and animals leads to excessive residue of SMX in wastewater and surface water, which leads to resistance genes in human body [7–9]. Residual antibiotics have a bullheaded inhibitory effect on microorganisms; therefore, traditional biochemical treatments cannot achieve the desired treatment effect. It is urgent to exploit effective methods to deal with antibiotic residues in the water environment.

Advanced oxidation processes (AOPs) are currently recognized as one of the most effective treatment methods for degrading toxic pollutants, which can replace the traditional process, and have been widely used in dyes [10], drugs, pesticides and other refractory organic organics [11–14]. Persulfates are a stable oxidant, which is convenient for storage and transportation, and it lays a foundation for the practical application of persulfate advanced oxidation process [15–17]. Peroxymonosulfate (PMS) and persulfate (PS) are two different persulfates that can provide free radicals $SO_4^{\bullet-}$, $^{\bullet}OH$, and singlet oxygen $^1O_2$; thereinto PMS is more likely to be activated. The stability and a redox potential of 2.5–3.1 V of $SO_4^{\bullet-}$ are slightly better than that of hydroxyl radicals ($^{\bullet}OH$ with 1.8–2.7 V) and $^1O_2$ (2.2 V) [18–21]. What is more to be expected is its positive oxidation and independence of pH value. Therefore, the development of practical methods for PMS activation is urgent. At present, the activation methods of PMS mainly include thermal activation, alkali activation, ultrasonic activation, and transition metal ions activation [22–24]. The transition metal ions activation method is concerned for its simple operation and strong practicability [25–28]. Recently, a great deal of transition metal oxides and bimetallic oxide catalysts have been synthesized and applied [29]. Magnetic crystal MFe_2O_4 (M = Co, Mn, Cu, Ni, etc.) has been found to have excellent catalytic properties and has

been applied in such as the degradation and removal of organic pollutants in water [30, 31]. However, most of the metal oxides nano-sized catalysts have some shortcomings in the application of water purification, for instance, the difficulty of separation and the help of external energy [32, 33]. Recently, among the many nano-metal composites, iron-based bimetallic oxides have been widely used in the degradation and removal of organic pollutants in water due to their strong magnetics [34–36]. Cobalt is the best of all transition metals for PMS activation; nevertheless, cobalt has shortcoming in practical water purification applications on account of its recognized carcinogenicity, high price and difficulty to recycle. So some researches turned to transition metal manganese which can also high efficient activate PMS in many degradation processes [37, 38]; however, the effect of manganese in bimetallic oxides on the catalyst performance is worth further study.

Inspired by most of the researches, magnetic bimetallic oxide porous manganese ferrite nanoparticles ($Mn_xFe_{3-x}O_4$) were synthesized with a simple hydrothermal method and applied to activate PMS for the degradation of SMX in this work. The porous structure of the prepared porous $Mn_xFe_{3-x}O_4$ was increased, and the activity of the catalyst was improved by calcining at high temperature. The reactive activation of $Mn_xFe_{3-x}O_4$ was compared with that other different Mn/Fe stoichiometric ratios catalysts and investigated under a variety of external conditions. The mineralization of SMX was determined by simultaneously observing the total organic carbon (TOC) detection and the formation of ammonia nitrogen. Free radical quenching experiments combined with EPR tests proved the generation of two kinds of free radicals, $SO_4^{\bullet-}$ and $^{\bullet}OH$, and singlet oxygen $^1O_2$ with the loadings of catalyst and concentrations of PMS in the degradation process and revealed their relative concentration changes ($SO_4^{\bullet-}$ and $^{\bullet}OH$, and $^1O_2$) under crescent conditions. The possibility of reusing of catalyst $Mn_xFe_{3-x}O_4$ was verified by measuring the concentration of iron and manganese ions in the solution after the reaction. Finally, the degradation pathways of sulfamethoxazole by magnetic porous manganese ferrite nanoparticles ($Mn_xFe_{3-x}O_4$) were determined according to the composition of the reaction products in the degradation system.

Materials and methods

Chemicals and reagents

PMS (Oxone [$KHSO_5 \cdot 0.5\ KHSO_4 \cdot 0.5\ K_2SO_4$, molecular weight: 307.38 g/mol]) was purchased from Sigma-Aldrich. $FeCl_3 \bullet 6H_2O$, $MnCl_2 \bullet 4H_2O$, sodium acetate anhydrous NaN_3 are purchased from China National Medicines Corporation Ltd. Sulfamethoxazole (SMX, 99%), ethylene glycol, polyethylene glycol (PEG) with 1000 MW, ethyl alcohol, methanol, tert-butanol, NaN_3, 5,5-dimethyl-1-pyrroline N-oxide (DMPO, 99%), 4-amino-2,2,6,6-tetramethylpiperidine (TEPM, 99%) are purchased from Aladdin. A certain concentration of PMS solution was prepared in advance for later dilution for degradation experiments. All other chemicals and reagents are not processed before use after purchase.

Synthesis of $Mn_xFe_{3-x}O_4$ catalysts

$Mn_xFe_{3-x}O_4$ was prepared by modified hydrothermal method and then calcined. $FeCl_3 \bullet 6H_2O$ and $MnCl_2 \bullet 4H_2O$ provide raw material sources of copper and iron. Manganese (II) and iron (III) with different molar ratios (0.1:2.9, 0.5:2.5, 0.7:2.3, 1.0:2.0, and 1.5:1.5) (abbreviated to $Mn_xFe_{3-x}O_4$ in the following article) are dissolved in 80 mL of ethylene glycol, and when they were completely dissolved, add 6.0 g sodium acetate anhydrous and 3.0 g PEG 1000 to the solution. Closely followed by 45 min of forceful stirring, the solution was poured into 100 mL Teflon-lined stainless steel autoclave at 200 °C for 8 h in oven. The resulting black—brown solid was dried in oven at 60 °C for 6 h after washed alternately with ethanol and water three times each using sucked out with a magnet, as reported in previous work of our research group [39]. The catalyst $Mn_xFe_{3-x}O_4$ spherical spinel was obtained by calcining at 450 °C in a muffle furnace for 3 h at the rate of 3 °C/min.

Characterization of $Mn_xFe_{3-x}O_4$ catalysts

The surface morphology and microstructure of obtained powder were observed by a field-emission scanning electron microscopy (SEM, FEI Quanta 200 FEG) and transmission electron microscopy (TEM, JEOL JEM-2010). The EDS pattern was analyzed with ZEISS Auriga SEM/FIB Crossbeam System. Fourier transform infrared (FTIR) spectrometer in KBr pellets

on a Thermo Nicolet Nexus-870 spectrophotometer was used to support the composition information of catalysts. Magnetite properties of the eventual products were measured using superconducting quantum interference device (Quantum Design MPMS XL5) in 300 K. Thermo-gravimetric analysis (TGA, SDT Q600) was characterized only in detecting the thermal stability of the catalysts. XRD analysis was performed using a PANalytical X'Pert instrument with a Cu Ka radiation. X-ray photoelectron spectroscopy (XPS, Thermo-VG Scientific ESCALAB 250) was used to investigate the catalysts before and after degradation.

Degradation experiments

All degradation experimental systems were completed containing $Mn_xFe_{3-x}O_4$ placed into a shaker with a speed of 200 rpm at room temperature (25 ± 2 °C) in 250-mL conical flask covered with tin foil to avoid light with SMX initial concentration 20 mg/L at pH 7.0 (by adjusting with 1.0 M NaOH and 1.0 M HCl). To explore the activity of five different catalysts, 0.20 g/L $Mn_xFe_{3-x}O_4$ were added separately into degradation systems under the same conditions after adding 60 mL SMX (initial concentration of 50 mM) and 20 mL PMS (initial concentration of 30 mM) in succession. In addition, a certain volume of SMX and PMS were added to dilute the concentration to 20 mg/L and 1–10 mM (1, 2, 4, 10 mM), and different amounts of catalysts (0.01–0.50 g/L $Mn_{1.5}Fe_{1.5}O_4$) were added to start the degradation experiment. The stability and repeatability of the $Mn_xFe_{3-x}O_4$ were observed by six cycle degradation experiments under the same above experimental conditions. All the experimental data of SMX degradation experiment were the average of three times by UV–Vis spectrophotometer (Fig. S1), and the error of experiments was reflected in the error bar of data graphs.

Kinetics were analyzed using the pseudo-first-order and pseudo-second-order model using Eqs. 1 and 2 [40]

$$C_t/C_0 = \exp(-k_1 t) \qquad (1)$$

$$1/C_t - 1/C_0 = k_2 t \qquad (2)$$

where C_0 express initial concentration, and C_t is the concentration at time t min of SMX (mg/g) in the $Mn_xFe_{3-x}O_4$/PMS system. k_1 (min^{-1}) and k_2 (g/mg min) are the pseudo first-order and pseudo second-order rate constants.

Degradation of sulfamethoxazole in real water samples was a formidable challenge; thus, the volume of the experimental system was designed to 1 L. A small Fenton tower device was structured with simulated actual water samples (0.20 g/L $Mn_{1.5}Fe_{1.5}O_4$, 20 mg/L SMX, 4.0 mM PMS, pH = 7.0, 10 mg/L Na^+/Mg^{2+} and 30 mg/L NO_3^-).

Analytical methods

Inductively coupled plasma atomic emission spectrometer (ICP PERKINELMER Optima 7300 DV) was used to measure the concentration of Mn and Fe ions in the reaction solution. In order to study and discuss conceivable degradation pathways, Agilent 6540 UHD accurate-mass quadrupole time-of-flight tandem mass spectrometer (Q-TOF-MS) with an electrospray ionization source was used to detect the mass of products and by-products generated in the degradation process of SMX. The mineralization of SMX was analyzed by detecting NH_4^+ (ammonia nitrogen) and TOC after degradation using $Mn_xFe_{3-x}O_4$/PMS [41].

The decrease of TOC in degradation system represents the mineralization of SMX, and the calculation method of mineralization degree is as follows Eq. 3:

$$\text{Mineralization degree} = TOC_t/TOC_0 \times 100\% \qquad (3)$$

where TOC_t and TOC_0 represent total organic carbon concentration after t minutes and initial organic carbon content of SMX.

Quenching experiments and EPR experiments

In order to analyze the production and predominance of free radicals $SO_4^{\bullet-}$, $^\bullet OH$ and non-free radical $^1O_2$ in $Mn_xFe_{3-x}O_4$/PMS degradation system, three quenching agents, methanol (MeOH), tert-butyl alcohol (TBA) and NaN_3 were added to the reaction system for comparison experiments. Previous studies reported that the quenching ability of MeOH to $SO_4^{\bullet-}$, $^\bullet OH$ was basically the similar, and TBA could quench $^\bullet OH$, and NaN_3 quench $^1O_2$ efficiently with the rate constants k_{MeOH}, $SO_4^{\bullet-}$, k_{MeOH}, $^\bullet OH$, k_{TBA}, $^\bullet OH$ and k_{NaN3}, $^1O_2$ shown in Table 1. Thereinto concentrations of MeOH and TBA were 100 mM and

Table 1 Second-order rate constant of quencher and oxidizing substances

Quenching agent	Free radicals and singlet oxygen species	Second-order rate constant $(L \times mol^{-1} \times s^{-1})$
MeOH	$^{\bullet}OH$	$(1.2–2.8) \times 10^9$
	$SO_4^{\bullet-}$	$(1.1–2.5) \times 10^7$
TBA	$^{\bullet}OH$	$(3.8–7.6) \times 10^8$
	$SO_4^{\bullet-}$	$(4.0–9.1) \times 10^5$
NaN$_3$	$^1O_2$	$7.8 \times 10^8–2.2 \times 10^9$
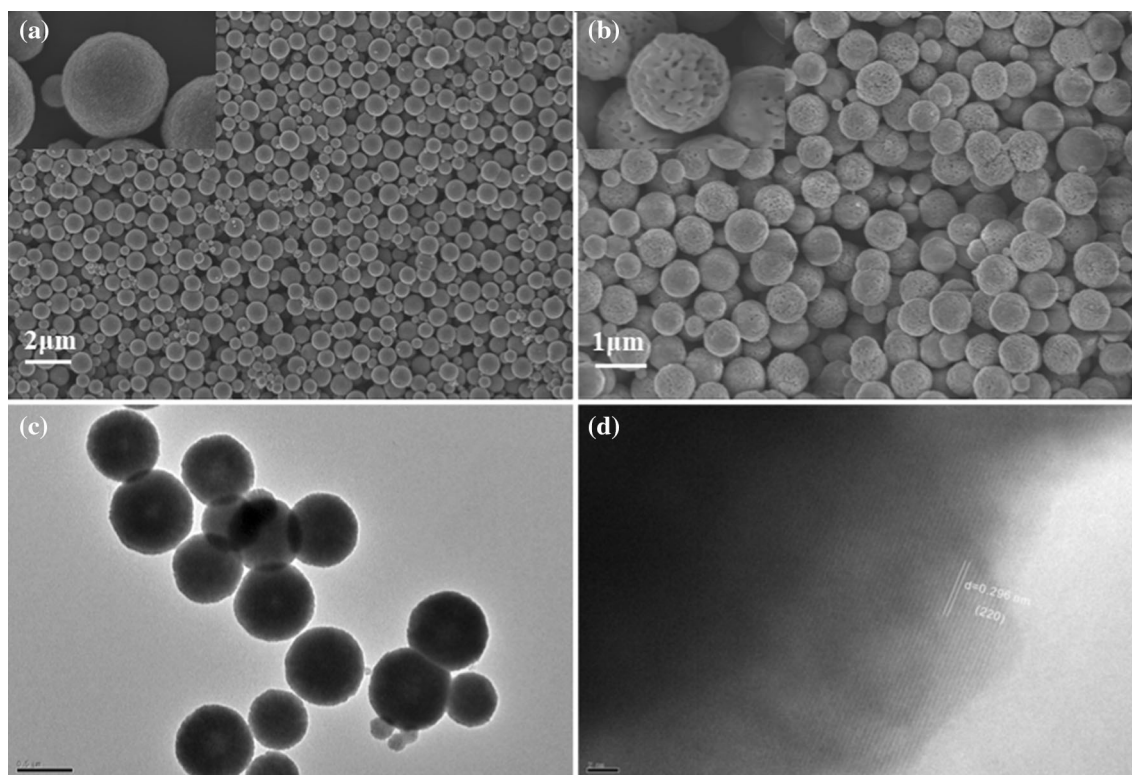
Figure 1 Characteristics of the synthesized magnetic porous manganese ferrite nanoparticles($Mn_xFe_{3-x}O_4$) catalysts: **a, b** SEM before and after calcination at 500 °C, **c** TEM, **d** HRTEM.

NaN$_3$ was 20 mM, and other experimental conditions are controlled as the best conditions of the above research. The types of free radicals $SO_4^{\bullet-}$, $^{\bullet}OH$ and singlet oxygen $^1O_2$ were proved by EPR (electron paramagnetic resonance) test using a spin-trapping agents DMPO and TEMP respectively by EPR (EMX 10/12, Bruker, Germany) at a resonance frequency of 9.39 GHz, microwave power of 5.02 mW, modulation amplitude of 0.30 G, receiver gain of 1.0 $\times 10^4$/2.0 $\times 10^4$, and regulatory sweep width, time constant and sweep time. Pre-weighed catalyst and a certain volume of PMS and SMX were added to 15-mL centrifugal tube, and capture agents DMPO (100 mM) and TEMP (100 mM) were added at the end. The

Table 2 EDS of $Mn_xFe_{3-x}O_4$ with different Mn/Fe stoichiometry

Percentage of elements

Catalysts	C	O	Mn	Fe
$Mn_{0.1}Fe_{2.9}O_4$	0.06	58.22	0.53	41.19
$Mn_{0.5}Fe_{2.5}O_4$	0.07	60.34	1.08	38.51
$Mn_{0.7}Fe_{2.3}O_4$	0.09	62.78	1.48	35.65
$MnFe_2O_4$	5.39	57.96	2.84	33.81
$Mn_{1.5}Fe_{1.5}O_4$	6.52	60.71	2.99	29.78

relative strengths of $SO_4^{\bullet-}$, $^{\bullet}OH$ and $^1O_2$ were detected under different loadings of catalysts
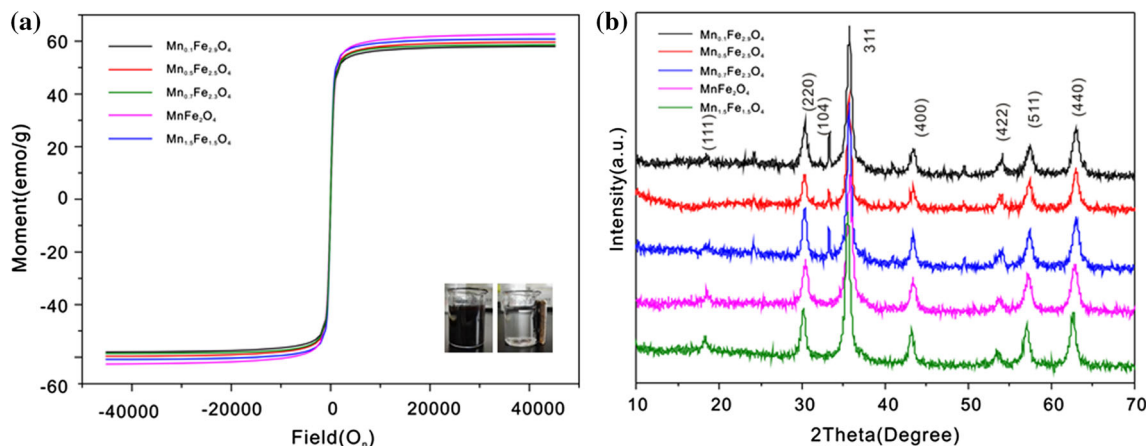
Figure 2 **a** Magnetic hysteresis loops, **b** XRD of $Mn_xFe_{3-x}O_4$.

$(0.01–0.50$ g/L $Mn_{1.5}Fe_{1.5}O_4)$ and concentrations of PMS $(1–10$ mM$)$.

Results and discussion

Characterization of $Mn_xFe_{3-x}O_4$ nanoparticles

All five $Mn_xFe_{3-x}O_4$ catalysts range in size by SEM and TEM from 500 to 600 nm with stable solid spherical structures. It was obvious that a mass of pores were formed on the surface of the catalyst after calcination at 450 °C (Fig. 1a and b), and they are favorable for the catalyst to contact with SMX to be degraded. However, the material size remains essentially unchanged before and after calcination. After calcination in high temperature, the internal structure of the material becomes less granular and more stable reflected in TEM (Fig. 1c) and HRTEM (Fig. 1d), the lattice spacing of 0.296 nm corresponds to the (220) planes of $Mn_xFe_{3-x}O_4$, consistent with the previous reports, which is beneficial to the degradation and multiple utilization of SMX. The EDS results confirm that the catalysts contain Mn, Fe, O and a small amount of C and the manganese relative amount in $Mn_xFe_{3-x}O_4$ increased with the increase of the Mn/Fe stoichiometry ratios (Table 2).

The observed field dependence the $Mn_xFe_{3-x}O_4$ catalysts agrees well with the reported room temperature superparamagnetic behavior of $MnFe_2O_4$ nanoparticle. The saturation magnetization of the $Mn_xFe_{3-x}O_4$ catalysts shown in Fig. 2a ranges from 57.53 to 62.79 emu/g. Among them, the catalyst with the strongest magnetic is $Mn_{1.5}Fe_{1.5}O_4$.

Superparamagnetic characteristics are beneficial for separation applications in water environments [42]. The XRD diffraction data of the synthesized catalysts $Mn_xFe_{3-x}O_4$ showed that they belong to the nanocrystal structure (Fig. 2b). The diffraction peaks were absolutely matched against the diffraction files of the JCPDS card No. 65–3107 indexed to synthetic spinel crystalline structure Fe_3O_4. And the peaks were at 18.34°, 30.28°, 35.7°, 43.39°, 54.05°, 57.41°, and 62.96° correspond to crystal planes (111), (220), (311), (400), (422), (511), and (440), respectively. The peak observed at 33.15° of $Mn_{0.1}Fe_{2.9}O_4$, $Mn_{0.5}Fe_{2.5}O_4$ and $Mn_{0.7}Fe_{2.3}O_4$ was assigned to little α-Fe_2O_3 produced during the synthesis process, which correspond to crystal planes (104) (JCPDS NO. 33-0664) [43, 44]

In FTIR spectra (Fig. S2a) of $Mn_xFe_{3-x}O_4$, metal oxide characteristic peak signals of catalysts are less than 1000 cm^{-1}, and the peaks at 438 and 578 cm^{-1} are corresponded to the stretching vibrations of Fe–O and Mn–O in the apparent spinel structure. The two high intensity peaks 3440 and 1644 cm^{-1} are recognized as hydroxyl groups. The spinel structure of all catalysts natures were confirmed once again. Fig. S2b showed N_2 adsorption–desorption isotherm and pore size distribution (inset) of $Mn_xFe_{3-x}O_4$. Compared with other MFe_2O_4 (M = Cu, Mn) prepared by predecessors [45, 46], the $Mn_xFe_{3-x}O_4$ possessed a higher specific surface area (47.55 m^2/g). The average pore diameter was 6.66 nm suggesting the mesoporous structure of catalysts. The larger specific surface area facilitated the affinity between the active sites on the catalysts surface and the corresponding substances to be activated.
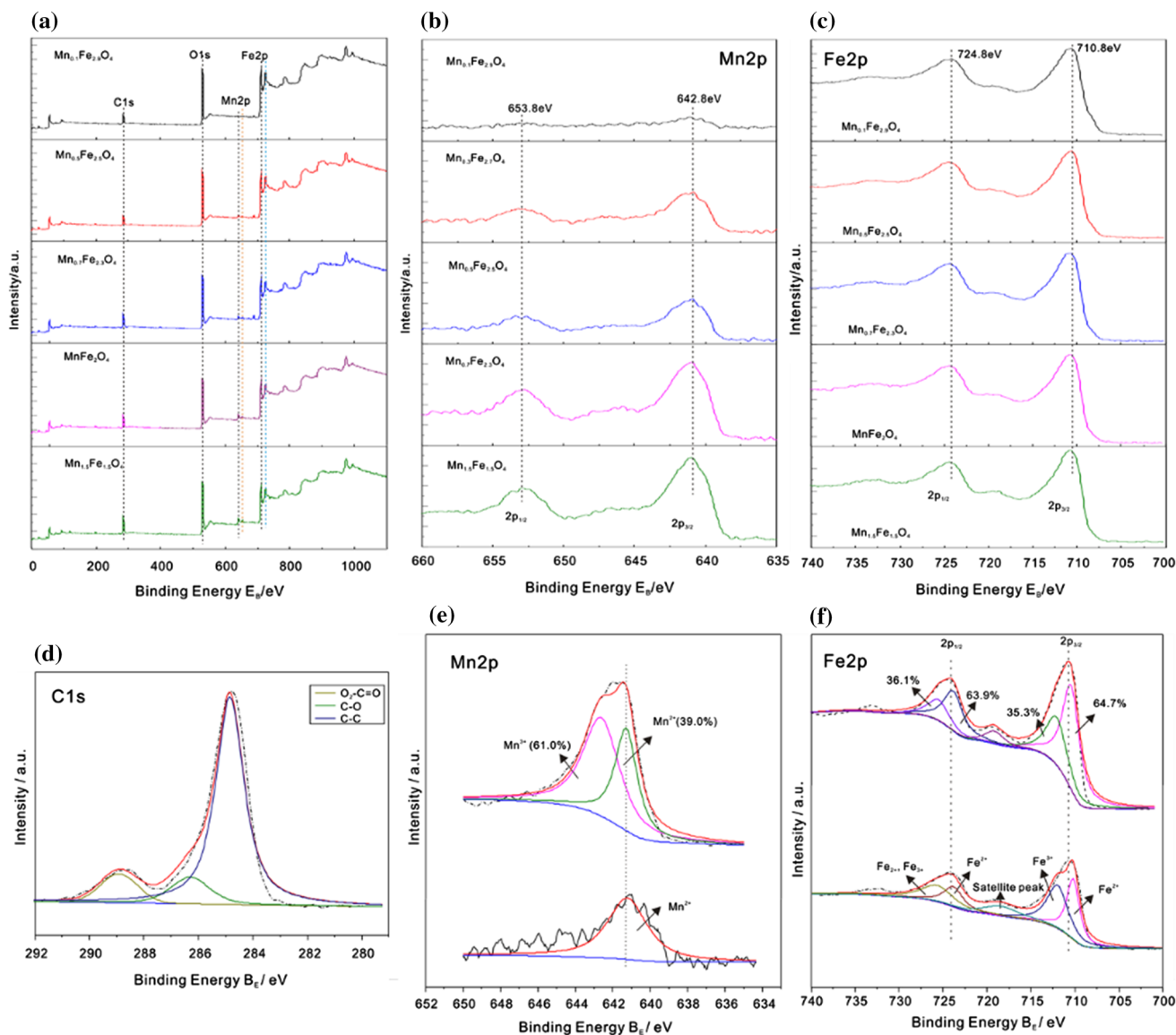
Figure 3 XPS spectra: **a** Survey scans, **b**, **e** Mn2p XP core level, **c**, **f** Fe2p XP core level, **d** deconvoluted C1s XP core level from $Mn_xFe_{3-x}O_4$.

TGA analysis was performed to investigate the $Mn_xFe_{3-x}O_4$ catalysts pyrolysis process, and the results were exhibited in the Fig. S3. The first mass loss (2.910%) processes that occurred between room temperature and 165.33 °C was assuredly derived from the weight of physically adsorbed water; next, the second mass losses (5.728%) in the range from 165.33 to 449.87 °C belonged to surface hydroxyl group namely chemisorption water. It followed that the structures and properties of the $Mn_xFe_{3-x}O_4$ catalysts were stable, which were conducive to the following long-term degradation experiments.

The XPS shows the elemental composition of the catalysts $Mn_xFe_{3-x}O_4$. The four predominant peaks on behalf of the Mn2p, Fe2p, O1s and C1s are clearly observed at about binding energy of 641.61, 711.26, 531.26 and 285.51 eV, respectively, in the spectrogram (Fig. 3a). Figure 3d displays XPS data of the C1s core level peak. The peak consists of three components assigned to O–C = O, C–O, and C–C bonds at 288.90 eV (I), 286.30 eV (II), ∼284.80 eV (III), respectively. These peaks were very intense in the $MnFeO_4$ sample. The C1s peak shape is characteristic of iron carbonate, $FeCO_3$ [47]. The C1s peak is less intense in the other three samples of cobalt ferrites
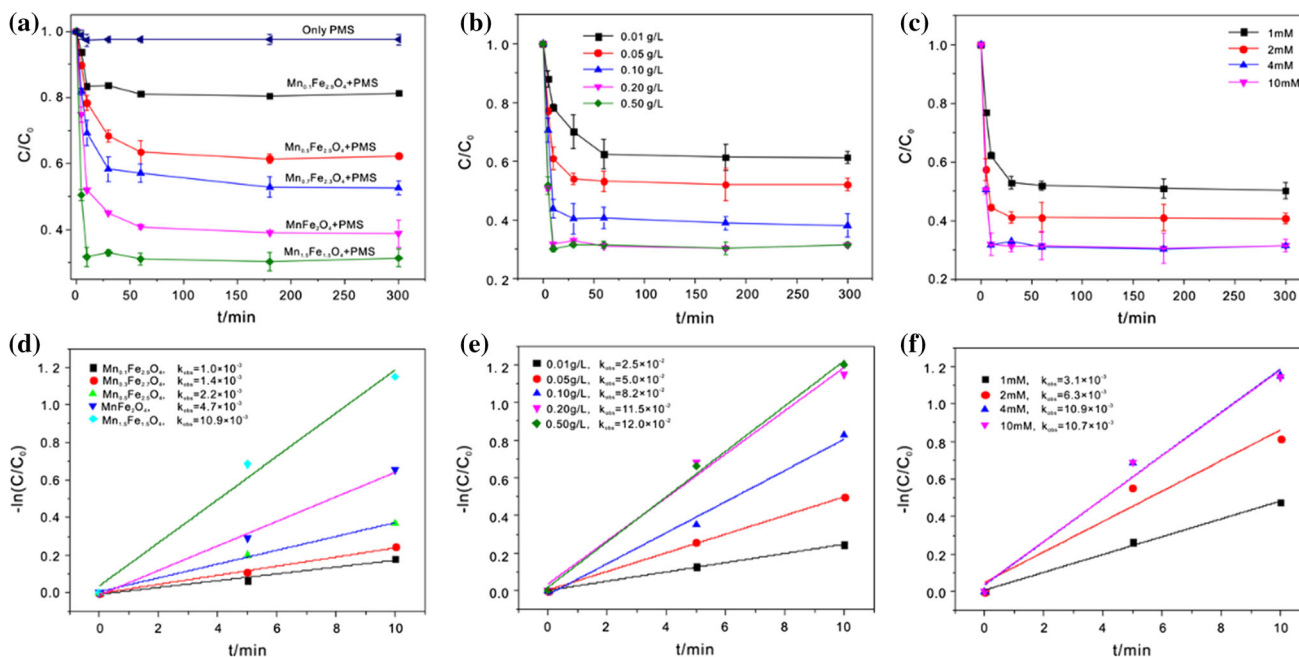
Figure 4 Effect of initial conditions on degradation of SMX by $Mn_xFe_{3-x}O_4$: **a** different molar ratios:0.1:2.9, 0.5:2.5, 0.7:2.3, 1.0:2.0, 1.0:1.0, **b** catalyst loadings, **c** catalyst concentrations of PMS, **d**–**f** pseudo-second-order kinetic models fitting. Other experimental parameters: C_0 = 20 mg/L, pH = 7.0, (a) 0.20 g/L $Mn_xFe_{3-x}O_4$, 4 mM PMS, (b) 4.0 mM PMS, (c) 0.20 g/L $Mn_{1.5}Fe_{1.5}O_4$.

[41, 48]. The XPS spectra of Mn2p as Fig. 3b of $Mn_xFe_{3-x}O_4$ showed the same form and binding energies and peaks of increasing strength are also consistent with the five catalysts with the relative increase of Mn dosage in the raw materials. The peak at 642.8 and 653.8 eV assigned to $Mn2p_{3/2}$ and $Mn2p_{1/2}$ [49], and the peak of Mn2p is not obvious due to the relatively low dosage in $Mn_{0.1}Fe_{2.9}O_4$. Figure 3e shows that Mn^{2+} existed on the surface of preparative catalysts unused [49, 50]. Figure 3c shows the XPS spectra of Fe2p, and it behaved differently from Mn2p, the peak area of Fe changed negligibly consistent with $Fe2p_{1/2}$ and $Fe2p_{2/3}$ in the binding energies of 724.8 and 710.8 eV with the change of Mn/Fe stoichiometric. The peak of 710.7 eV was assigned to Fe^{2+} possibly derived from manganese ferrite or iron carbonates; furthermore, the peak with higher binding energy abound 712.1 eV had been assigned to Fe^{3+} from ferric oxide (Fig. 3f) [50, 51].

Degradation of SMX using $Mn_xFe_{3-x}O_4$/PMS

Effect of Mn/Fe stoichiometric ratio

The degradation degree of SMX was an important index to judge the activity of catalysts $Mn_xFe_{3-x}O_4$ (with different Mn/Fe molar ratios, 0.1:2.9, 0.5:2.5, 0.7:2.3, 1.0:2.0, and 1.5:1.5)/PMS. Figure 4a demonstrated SMX was hardly degraded in the reaction system with no catalyst as only existence of PMS under experimental conditions: 4 mM PMS, C_0 of SMX 20 mg/L, and 7.0 pH value. Moreover, the SMX was mostly degraded at a certain time after the subsequent addition of constant concentration PMS (4 mM) in the degradation system in which there was no degradation with only catalyst. PMS naturally occurred as an oxidant in degradation systems. At the same time, it was observed that the degradation results of five catalysts with the same mass ($Mn_xFe_{3-x}O_4$ 0.20 g/L) were completely different. The degradation efficiency of catalysts $Mn_xFe_{3-x}O_4$ also increased gradually with the increase of Mn/Fe relative stoichiometric ratio. In other words, removal efficiency of five catalysts was: $Mn_{1.5}Fe_{1.5}O_4$ (with a removal rate of

70%) > $MnFe_2O_4$ > $Mn_{0.7}Fe_{2.3}O_4$ > $Mn_{0.5}Fe_{2.5}O_4$ > $Mn_{0.1}Fe_{2.9}O_4$. Under the approximate reference conditions, the removal efficiency for SMX degradation of the porous $Mn_{1.5}Fe_{1.5}O_4$ catalyst was higher than that of most of the catalysts reported previously (Table S1).

And the degradation processes of catalysts conformed to pseudo-second-order kinetic models (Fig. 4d). In addition, it could be observed that in the catalysts and PMS system, SMX degraded rapidly in the initial 20 min, and then, the degradation efficiency of tended to be stable without obvious change. This behavior has been shown in many semblable catalytic studies. This phenomenon was caused by the commonly perceive catalyst "surface poisoning." In order to observe the best degradation efficiency under the influence of subsequent diverse experimental conditions, $Mn_{1.5}Fe_{1.5}O_4$ was examined with the best degradation rate (70%) of degradation of SMX among five catalysts. Another problem that we should pay attention to is that in the catalyst and PMS degradation of SMX system, there may be slight changes in the pH of the solution caused by the mixture of two solutions (SMX and PMS), and we did not consider the influence on the experiment, which is more conducive to the different test conditions existing in our actual water samples.

Effect of $Mn_xFe_{3-x}O_4$ loadings and concentrations of PMS

Considering that degradation experiments may be affected by many environmental factors, the influences of different loadings of $Mn_{1.5}Fe_{1.5}O_4$ and PMS at different concentrations on SMX degradation were described in Fig. 4b and c. On the one hand, the degradation was observed for 300 min at 20 mg/L initial concentration of SMX, 4 mM PMS and pH = 7.0. The removal rate of SMX increased gradually from 37 to 70% (with catalyst loadings from 0.01 to 0.50 g/L) with the pseudo-second order reaction rate constants (k_{obs}) increased from 0.0246 to 0.1201 min^{-1} (Fig. 4e); nevertheless, when the catalysts loading increased to the 0.50 g/L, the degradation rate of SMX decreased compared with the previous maximum removal rate. It might be well understood that when the loadings of the catalyst $Mn_{1.5}Fe_{1.5}O_4$ was increased, it could promote the activation of PMS to produce more strong oxidizing substances and increase the degradation of SMX. While, when the loading exceeded a certain amount, the exposed
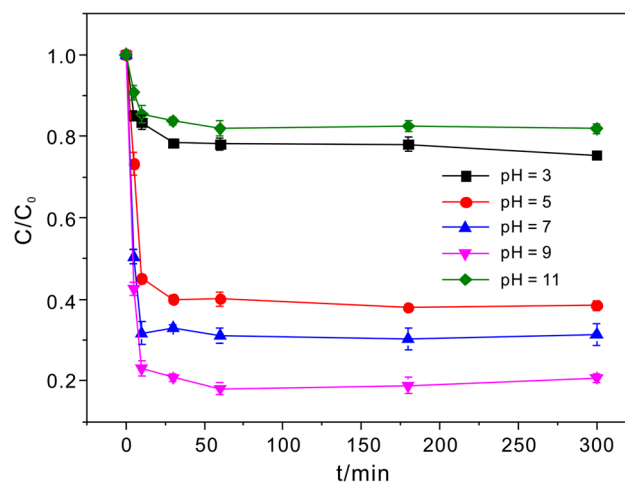

Figure 5 Effects of solution pH on the SMX degradation process in $Mn_{1.5}Fe_{1.5}O_4$/PMS systems. Other experimental parameters: C_0 = 20 mg/L, 4.0 mM PMS, 0.20 g/L $Mn_{1.5}Fe_{1.5}O_4$, pH = 3–11.

surface of catalyst activated PMS was reduced because of the inherent agglomeration of the nanomaterial; therefore, the degradation of SMX was relatively stable or even reduced.

In the same way, similar to general perception, the increase of concentration of PMS was beneficial to the degradation of SMX. It was also intuitive to analyze the effect of PMS concentration on the removal of SMX by k_{obs} increasing from 0.0031 to 0.0110 min^{-1} with an 0.20 g/L $Mn_{1.5}Fe_{1.5}O_4$, 20 mg/L initial concentration of SMX (1.0, 2.0, and 4.0 mM), and pH = 7.0. Certainly, it was also apparent that the concentration of PMS further increased to 10 mM did not cause the degradation of SMX to increase
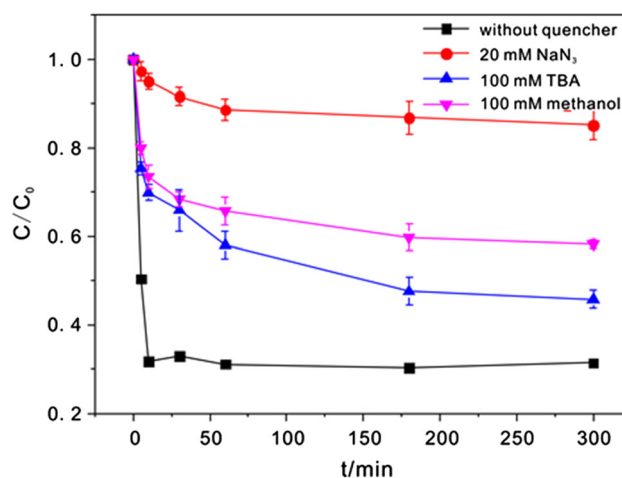

Figure 6 Effects of different quenching agents on degradation of SMX. Experiment conditions: 0.20 g/L $Mn_{1.5}Fe_{1.5}O_4$, 4.0 mM PMS, C_0 = 20 mg/L, pH = 7.0.

continuously but remained substantially constant with $k_{obs} = 0.011$ min^{-1} (Fig. 4f). It signified that when PMS exceeded a certain concentration, the loadings of Mn$_x$Fe$_{3-x}$O$_4$ was the main factor affecting degradation.

Effect of solution pH in Mn$_x$Fe$_{3-x}$O$_4$/PMS system

For field of environmental remediation, the influence of pH value is very important. Hence, the effect of solution pH ranges from 3 to 11 in Mn$_x$Fe$_{3-x}$O$_4$/PMS system of SMX degradation was investigated. As shown in Fig. 5, degradation efficiency was seriously negative affected in excessively acidic and alkaline solution. Effect of solution pH mainly depended on deprotonation of oxidant and surface charges of Mn$_x$Fe$_{3-x}$O$_4$ [52]. When the pH was adjusted to 3, the

oxidant PMS tended to break down to produce SO$_4^{2-}$ rather than SO$_4^{\bullet-}$. And at pH of 11, the production of SO$_5^{\bullet-}$ was reduced due to the deprotonation of PMS and it was not conducive to the affinity of negative groups HSO$_5^-$, SO$_5^{2-}$ on the surface of Mn$_x$Fe$_{3-x}$O$_4$ with negatively charged. Although the degradation efficiency of the catalysts was outstanding at a pH of 9, in order to make the catalysts better suited to the mild water environment, other parameters affecting of SMX degradation were selected under neutral condition (pH = 7).

Free radical quenching and EPR studies

It is well known that the types of oxidants that may occurred in the activation of PMS by catalysts Mn$_x$Fe$_{3-x}$O$_4$ include free-radical SO$_4^{\bullet-}$, $^\bullet$OH or singlet
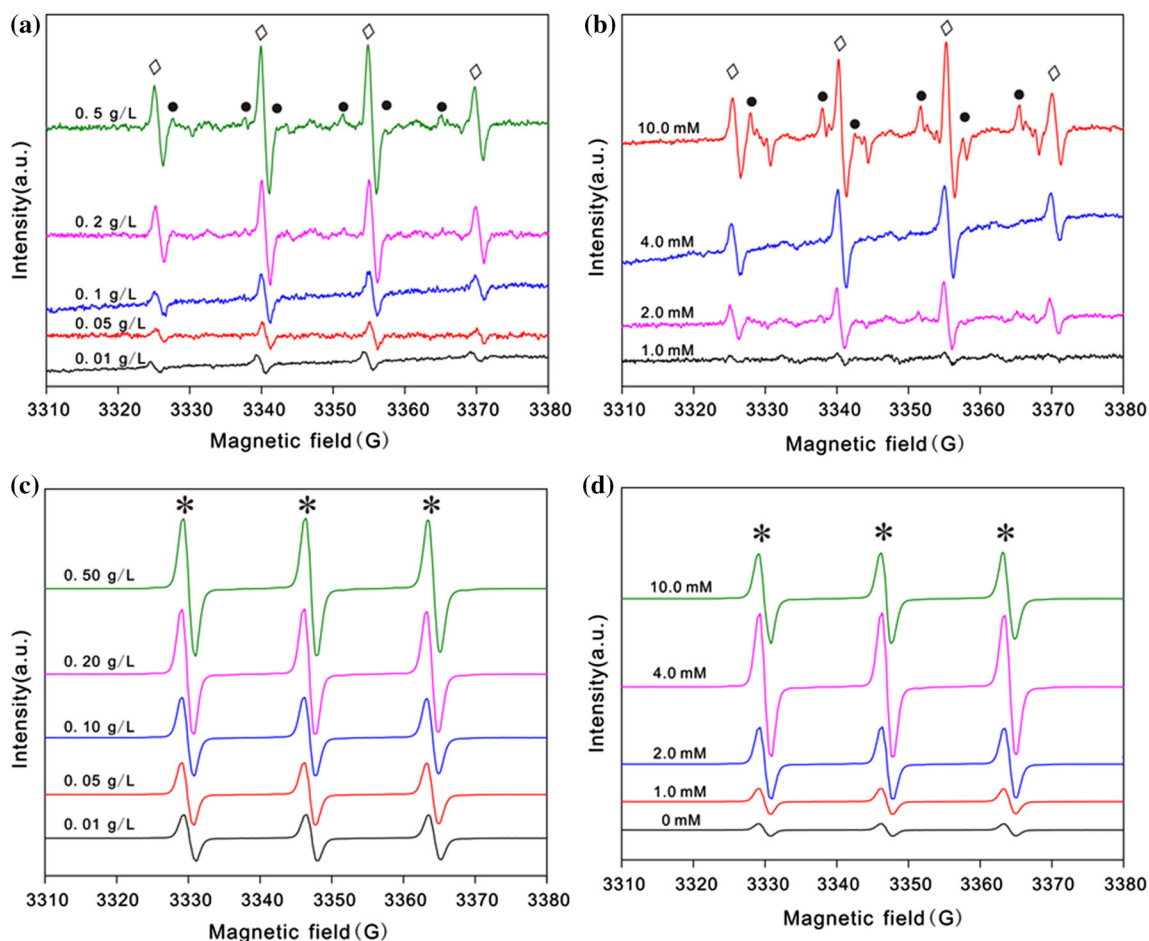
Figure 7 EPR of free-radical SO$_4^{\bullet-}$, OH$^\bullet$ of **a** Mn$_{1.5}$Fe$_{1.5}$O$_4$ loadings, **b** concentrations of PMS, and singlet oxygen of ^{1}O$_2$ **c** Mn$_{1.5}$Fe$_{1.5}$O$_4$ loadings, **d** concentrations of PMS generated in the PMS/ Mn$_{1.5}$Fe$_{1.5}$O$_4$ system. Experiment conditions: C$_0$ = 20 mg/ L, pH = 7.0, **a**, **c** 0.01, 0.05, 0.10, 0.20, 0.50 g/L Mn$_{1.5}$Fe$_{1.5}$O$_4$, 4 mM PMS, **b**, **d** 0.20 g/L Mn$_{1.5}$Fe$_{1.5}$O$_4$, 1, 2, 4, 10 mM PMS. Sulfate radicals (DMPO-SO$_4^{\bullet-}$: (●), hydroxyl radicals (DMPO-OH$^\bullet$: (◇) and (TMPO-^{1}O$_2$: (*) are denoted.

oxygen $^1O_2$. As shown in the Fig. 6, after adding of MeOH, TBA and NaN_3, the removal efficiency declined to 40%, 50% and 14%, respectively. These results showed that both $SO_4^{\bullet-}$, $^\bullet OH$ and $^1O_2$ contributed to the degradation of SMX and $^1O_2$ probably played a leading role. Because Eqs. 12 and 13 showed that $^\bullet OH$ was produced from $SO_4^{\bullet-}$ and H_2O/OH^-, the main responsibility for degradation of SMX is $SO_4^{\bullet-}$. For $^1O_2$, the self-decomposition of PMS and the promotion of the catalysts were not drastic, but the presence of plentiful hydroxyl groups accelerated the decomposition of PMS to $^1O_2$.

EPR experiments further verified the existence of three oxidants in the PMS activation process. The EPR provided a good explanation for the experiments to explore the influence of catalyst loadings and the different concentrations of PMS on degradation. Figure 7a and b shows that the signals of DMPO-$SO_4^{\bullet-}$ and DMPO-$^\bullet OH$ occurred in the activation of PMS by catalyst $Mn_{1.5}Fe_{1.5}O_4$, assigned according to their hyperfine splitting constants (DMPO-$SO_4^{\bullet-}$: $a_N = 13.2$ G, $a_H = 9.6$ G, $a_H = 1.48$ G, and $a_H = 0.98$ G; DMPO-$^\bullet OH$: $a_H = a_N = 14.9$ G) [53, 54]. And Fig. 7c and d described PMS activation also formed TEMP-$^1O_2$ signals with the hyperfine splitting constants (TEMP-$^1O_2$: $a_N = 16.9$ G) [55]. Results displayed that the peak intensity of EPR also increased gradually and remained invariable consistent followed aggrandizement of catalyst loadings or enhancement of concentration of PMS in accord with the degradation trend of SMX. AS shown in Fig. 7a and c, the peak intensity of EPR enlarged by four-

fold. With the catalyst loadings increased from 0.01 to 0.20 g/L, what's even more remarkable was that when catalyst loading was 0.50 g/L, the peak intensity increased nine-fold. Moreover, Fig. 7b and d shows that as the PMS concentration increased from 1 to 10 mM, the peak intensity of PMS also enlarged, but it was obvious that the effect was not as significant as on the catalyst loadings. In general, the analysis of quenching experiments and EPR indicated that catalysts $Mn_xFe_{3-x}O_4$ promoted the activation of PMS to produce free-radical $SO_4^{\bullet-}$, $^\bullet OH$ and singlet oxygen $^1O_2$ participating in the degradation of SMX.
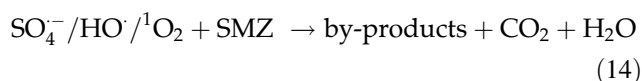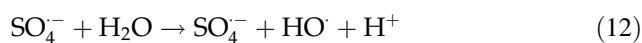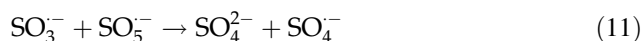
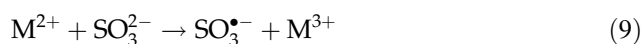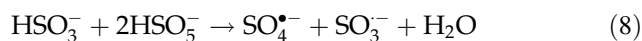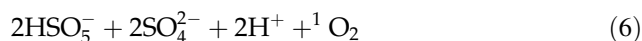### Activation mechanism of PMS on catalysts $Mn_xFe_{3-x}O_4$

It is well-known that free-radical $SO_4^{\bullet-}$, $^\bullet OH$ were main products by the transition metals activation of PMS mentioned in previous studies. However, in the degradation experiments, the role of transition metals Mn and Fe ions mainly served as activator for PMS, and the degradation of SMX was mainly dependent on not only strong oxidizing free-radical $SO_4^{\bullet-}$, $^\bullet OH$ but singlet oxygen $^1O_2$ produced by the activation process. And evidence of Mn and Fe ions participating in the activation were proved by the XPS spectra of the two metals before and after the degradation. Figure 3e displayed that Mn^{3+} (642.4 eV) accounted for 61.0% of Mn species. The deconvolution peaks of Fe2p were slightly shifted and dramatical increases of strength because of electron transfer. There were conspicuous changes in

Figure 8 Schematic illustration of the mechanism of PMS activation during SMX degradation.
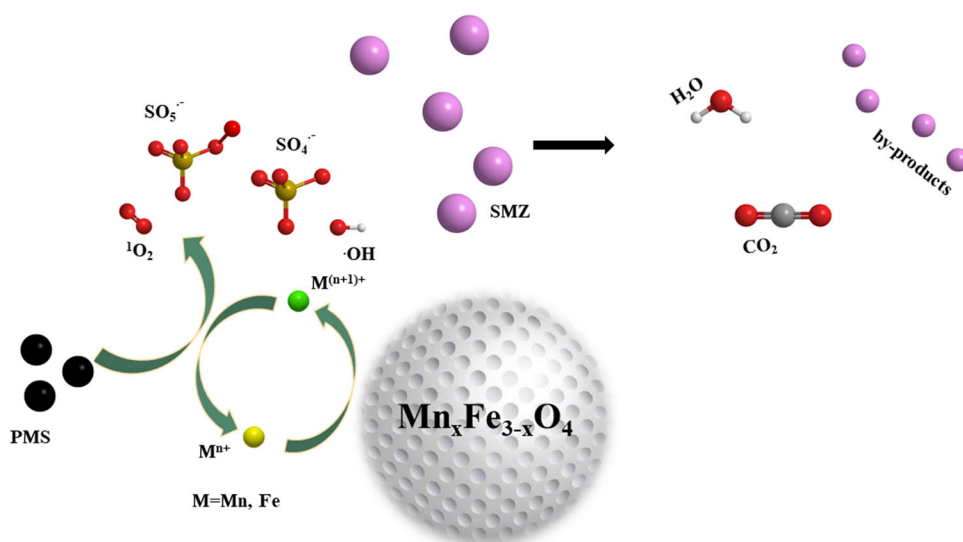
the peak area proportions of Fe^{3+} (712.1, 725.5 eV) and Fe^{2+} (710.5, 723.9 eV) in terms of the deconvolution peaks of $Fe2p_{1/2}$ and $Fe2p_{3/2}$ envelops after degradation as shown in Fig. 3f. It was verified that the transition metal Mn and Fe on the surface of the catalysts participated in the process of activating PMS to produce strong oxidizing substances for redox nature as illustrated in following Fig. 8 [49]. Also, the transition metals ion M^{2+} activated the hydrogen sulfate radical to produce $SO_4^{\bullet-}$ and $SO_5^{\bullet-}$ as shown in Eqs. 4 and 5. Equation 6 described the decomposition of PMS to produce $^1O_2$, and the addition of Mn/Fe also increased decomposition rate. The free radicals $SO_4^{\bullet-}$, $^\bullet OH$ (Eqs. 4–13) and singlet oxygen $^1O_2$ (Eq. 6) served as oxidants in the degradation system of SMX, which ultimately oxidized to degrade the SMX into CO_2, H_2O and by-products (Eq. 14).

$$M^{2+} + HSO_5^- \rightarrow M^{3+} + SO_4^{\cdot-} + OH^- / M^{3+} + SO_4^{2-} + HO^\cdot \tag{4}$$

$$M^{3+} + HSO_5^- \rightarrow M^{2+} + SO_5^{\cdot-} + H^+ \tag{5}$$

$$2HSO_5^- + 2SO_4^{2-} + 2H^+ + {}^1O_2 \tag{6}$$

$$HSO_5^- + SO_5^{2-} \rightarrow HSO_4^- + SO_4^{2-} + {}^1O_2 \tag{7}$$

$$HSO_3^- + 2HSO_5^- \rightarrow SO_4^{\bullet-} + SO_3^{\cdot-} + H_2O \tag{8}$$

$$M^{2+} + SO_3^{2-} \rightarrow SO_3^{\bullet-} + M^{3+} \tag{9}$$

$$SO_3^{\cdot-} + O_2 \rightarrow SO_5^{\cdot-} \tag{10}$$

$$SO_3^{\cdot-} + SO_5^{\cdot-} \rightarrow SO_4^{2-} + SO_4^{\cdot-} \tag{11}$$

$$SO_4^{\cdot-} + H_2O \rightarrow SO_4^{\cdot-} + HO^\cdot + H^+ \tag{12}$$

$$SO_4^{\cdot-} + OH^- \rightarrow SO_4^{\cdot-} + HO^\cdot \tag{13}$$

$$SO_4^{\cdot-} / HO^\cdot / {}^1O_2 + SMZ \rightarrow \text{by-products} + CO_2 + H_2O \tag{14}$$
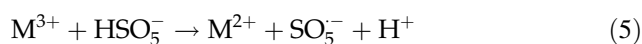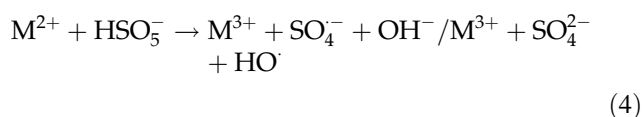
where M stands for transition metals Mn and Fe. Both M^{3+} metal ions in the catalysts played a certain role in activating PMS. The addition of Mn caused the acceleration of activation, and the removal efficiency increased with the enlargement of the relative stoichiometry of Mn, which also indicates that this understanding is reasonable.

Among the many equations (Eqs. 4 to 14), considering the redox potential of $HSO_5^-/SO_4^{\bullet-}$ (2.5 − 3.1 V) and $HSO_5^-/SO_5^{\bullet-}$ (1.1 V) and according to the reduction potential of the reduction of Fe^{3+}

Figure 10 Diagram of possible intermediates and degradation ▶ pathways in PMS/$Mn_xFe_{3-x}O_4$ system.

(0.77 V), we concluded that the regeneration of Fe^{2+} was the main rate limiting step.

To explore whether Fe is involved in activating PMS in addition to providing magnetic properties during the degradation process, we added a new control group for the SMX degradation of Fe_3O_4/PMS. The XRD, surface morphology and the reference experimental were shown in Fig. S4a. Obviously, when Fe_3O_4 without Mn was added into the degradation system (Fig. S4b), SMX was almost not degraded and the SMX removal rate increased significantly with addition of Mn. Because the redox cycle between Mn^{3+}/Mn^{2+} was thermodynamically favorable, we speculate Mn is the main active site on the catalyst surface combined with the performance of Fe_3O_4 in the degradation system. On the other hand, it is reported that the stability of complex between Fe and ligand is generally considered to be better than that of Mn and the modification of the stronger coordination environment between Fe and PMS increases the probability of producing free radicals. Therefore, we assumed that the synergistic effect between Fe and Mn was a decisive factor for activation of PMS.

Mineralization of SMX

The mineralization products of *C* and *N* in the system were explained by investigation of TOC, NH_4^+ and nitrate nitrogen (NO_3^-) in SMX solution after degradation. It had been reported that the nitrogen on the amino group was generally converted into
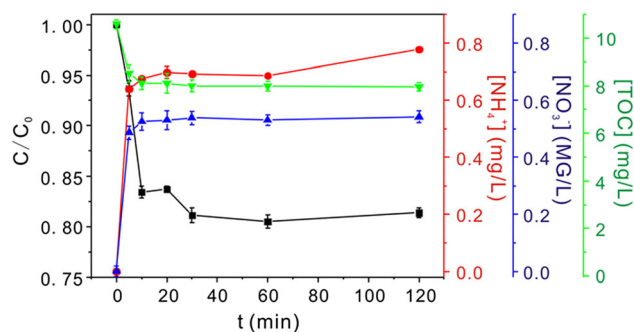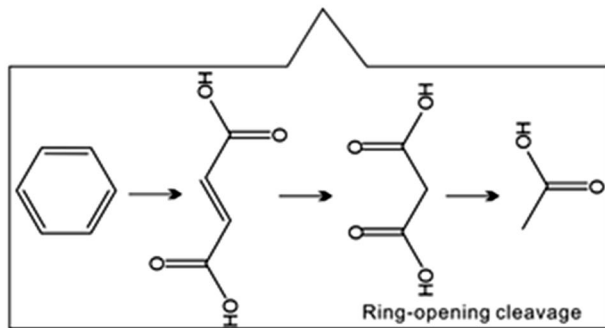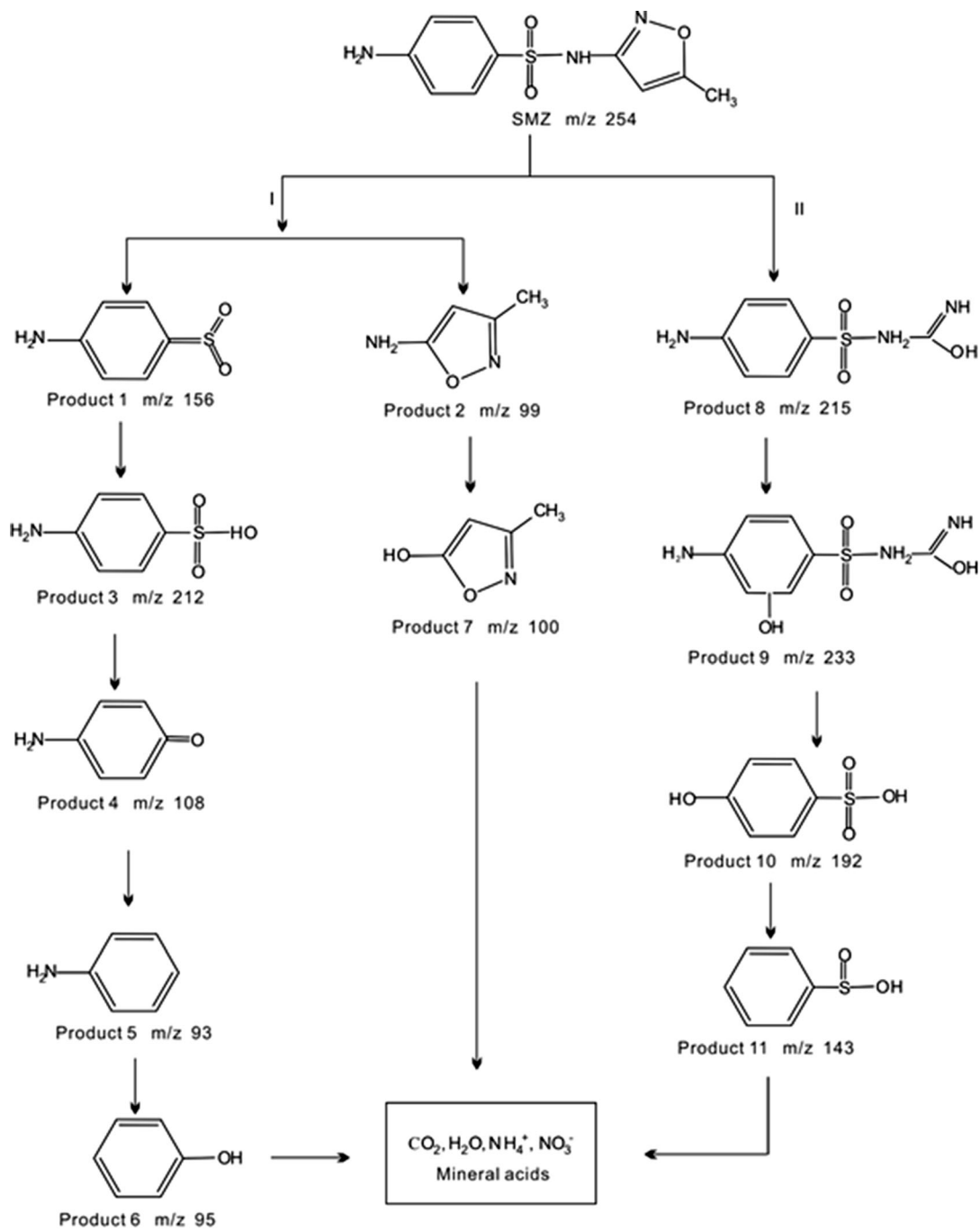

Figure 9 Mineralization degree of SMX and formation of NH_4^+ and NO_3^- in PMS/$Mn_xFe_{3-x}O_4$. Experimental conditions: 0.20 g/L $Mn_{1.5}Fe_{1.5}O_4$, 4 mM PMS, C_0 = 20 mg/L, pH = 7.0.

NH_4^+, and the nitrogen-containing heterocyclic ring of isoxazole was mostly converted into NH_4^+ and NO_3^- [56]. Figure 9 presented the conversion degrees of TOC, NH_4^+ and NO_3^-. Negligible TOC were reduced only 25% within 20 min and remained invariable for the following 2 h in the degradation of SMX system using PMS activated by $Mn_xFe_{3-x}O_4$ catalysts. It followed that the further mineralization of SMX required a longer reaction time. After 20 min of degradation, 0.69 mg/L NH_4^+ and 0.54 mg/L NO_3^- were detected, which was also synchronous with degradation of 70% SMX. In theory, few nitrite ions (NO_2^-) were released considering that NO_2^- was unstable in solution easily oxidized to NO_3^-. In general, SMX was mainly mineralized into ammonia nitrogen, nitrate nitrogen and trace amounts of nitrite in degradation systems.

Possible by-products and pathways for degradation of SMX

During the integrated degradation, target antibiotic SMX was subjected to different levels of hydroxylation, elimination of sulfonate group, oxidation of amino group and ring-opening cleavage mainly through the different attacks of free-radical $SO_4^{\bullet-}$, $^\bullet OH$ and singlet oxygen $^1O_2$.

Figure 10 demonstrated the SMX intermediates and the feasible two degradation pathways by LC–MS spectrogram (Fig. S5) during the degradation of antibiotic by PMS activated by $Mn_xFe_{3-x}O_4$. The appearance of the product with an m/z of 254 described the unreacted SMX molecules during degradation. The degradation pathway analysis mainly was owing to the first difference molecular sites to attack. Pathway I: As stated in previous reports, cleavage of S–N bond occurred easily in SMX [57], the cleavage of S–N bond resulted in SMX molecular resolved into product 1 (m/z of 156) and product 2 (m/z of 99). Certainly, product 1 quickly

converted to product 3 sulfanilic acid with m/z of 212. And then, sulfanilic acid naturally oxidized to hydroxyl sulfanilic acid. Subsequently, further decomposition of hydroxyl sulfanilic acid occurred to generate product 4 (m/z of 108) and following product 5 (m/z of 93), product 6 (m/z of 95) on account of the release of sulfonate group. Once again, the amino group on heterocyclic ring of product 2 was also oxidized to product 7 (m/z of 100) (the hydroxylation of benzene ring) which was cracked with ring-opening, and all products finally mineralized into CO_2, H_2O, NH_4^+, NO_3^- and mineral acids. Pathway II: Considering that hydroxylation might occur on heterocycle of SMX, the molecular structure of SMX could be reorganized to form derivatives. In consequence, heterocycle of SMX was oxidized and molecule cleaved to product 8 (m/z of 215) by structure reengineering with the subsequent hydroxylation – deamination (product 9 with m/z of 233) [58]. Product 10 (m/z of 192) and product 11 (m/z of 143) were generated resulting from cleavage of S–N bond and oxidation of amino group. Finally, the resulting simple molecules like benzene, phenol and so on were mineralized into CO_2, H_2O, NH_4^+, NO_3^- and mineral acids by ring-opening under the oxidation of attacks of free-radical $SO_4^{\bullet-}$, $^\bullet OH$ and singlet oxygen $^1O_2$.

Stability and reusability of $Mn_xFe_{3-x}O_4$

For environmental pollution governance, the choice of catalysts is particularly significance in excellent stability and reusability. On the one hand, the residual concentrations of Mn and Fe ions in the collected solution after degradation were detected by ICP-MS. The data showed that the concentrations of Mn and Fe ions in the solution after 1 h and 4 h degradation only were 0.063, 0.869, 0.091, and 1.076 μg/mL, respectively, 9 (Table 3). On the other hand, the analysis about FTIR of catalysts collected in the degradation system in Fig. 11a revealed that catalyst structure had not changed substantially after degradation. The degradation degree during the five cycle degradation experiments indicated a gradually decreasing trend, but the overall degradation rate remained relatively high as shown in Fig. 11b. The loss of metal ions might be responsible for activation of PMS generating oxidizing substances and the production of some "toxic" substances probably were the leading causes in multiple degradation systems.

Table 3 The concentrations of residual of Fe and Mn ions in solution systems after 1 and 4 h degradation of SMX, respectively, by ICP-MS

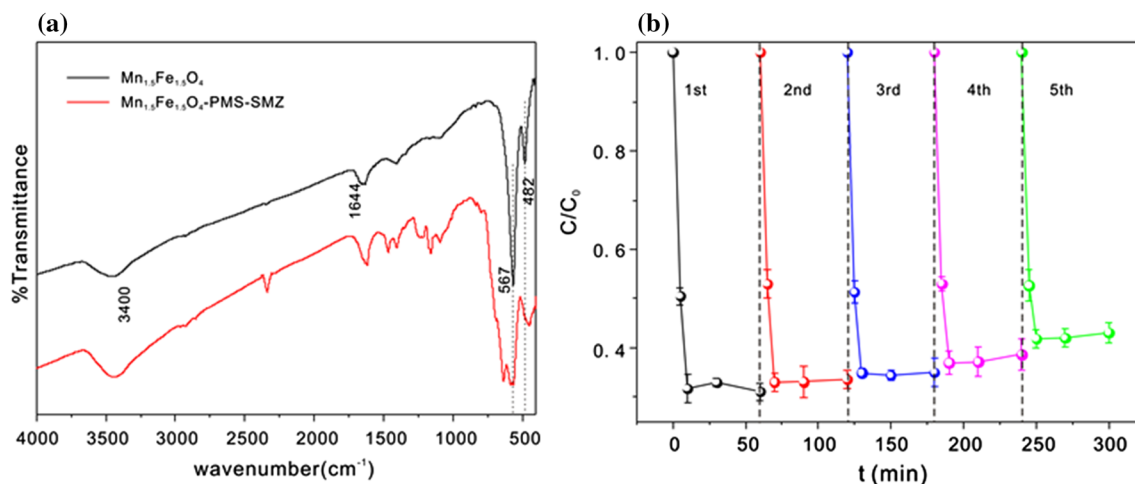| Time (h)	Fe (μg/mL)	Mn (μg/mL)
1	0.869	0.063
4	1.076	0.091

Figure 11 **a** FTIR spectra of $Mn_{1.5}Fe_{1.5}O_4$ before and after the degradation experiment, **b** Degradation of SMX during five different batch runs using $Mn_{1.5}Fe_{1.5}O_4$.

Scale-up experiment test

As shown in the Fig. S6, the $Mn_{1.5}Fe_{1.5}O_4$/PMS system still maintained a certain degradation performance in simulated actual water samples. The degradation efficiency reached 45% after 60 min in the water environment with overloaded interfering ions concentration. Therefore, it was speculated that the catalyst would make an excellent candidate in the actual water sample.

were deduced by LC–MS analysis of intermediate including: (I) cleavage of the S–N bond; (II) hydroxylation of benzene and heterocyclic ring; (III) disappearance of sulfonate group; (IV) oxidation of amino group; (V) ring-opening cleavage. Finally, the $Mn_x Fe_{3-x}O_4$ catalysts showed good stability and reuse performance after five cycle experiments. The magnetic $Mn_x Fe_{3-x}O_4$ catalysts have inestimable potential in environmental repair and pollutants degradation due to their excellent stability and reuse performance.

Conclusion

The magnetic porous manganese ferrite nanoparticles($Mn_x Fe_{3-x}O_4$) catalysts were prepared by a common hydrothermal method followed by calcining at a certain temperature according to different Mn/Fe stoichiometry. In this study, a deep insight and analysis in activation PMS using $Mn_x Fe_{3-x}O_4$ for degradation of SMX antibiotics were presented. The $Mn_{1.5}Fe_{1.5}O_4$ showed great degradation degree (70%) of SMX after 10 min with 4 mM PMS for 20 mg/L initial concentration at pH 7.0 of SMX. SMX was mainly degraded into CO_2, H_2O, NH_4^+, NO_3^- and mineral acids, and the TOC was reduced by 20%. Mn and Fe ions in the activation of PMS promoted each other and participated jointly in the activation, and the verification of EPR and quenching experiments revealed activation produced strong oxidizing substances free-radical $SO_4^{\bullet-}$, $^{\bullet}OH$ and singlet oxygen $^1O_2$ involved in degradation of SMX. Two possible degradation pathways of SMX in degradation system

Acknowledgements

Compliance with ethical standards

Conflict of interest The authors declare that they have no conflict of interest.

References

[1] Wang J, Liu W, Zhong D, Ma Y, Ma Q, Wang Z, Pan J (2019) Fabrication of bismuth titanate nanosheets with tunable crystal facets for photocatalytic degradation of antibiotic. J Mater Sci 54:13740–13752. https://doi.org/10.1007/s10853-019-03882-1

[2] Zhang R, Han Q, Li Y, Zhang T, Liu Y, Zeng K, Zhao C (2019) Fabrication and characterization of high efficient Z-scheme photocatalyst Bi_2MoO_6/reduced graphene oxide/BiOBr for the degradation of organic dye and antibiotic under visible-light irradiation. J Mater Sci 54:14157–14170. https://doi.org/10.1007/s10853-019-03883-0

[3] Vaizoğullar Aİ (2020) An effective photocatalytic and photoelectrochemical performance of $β/γ$-MnS/CdS composite photocatalyst for degradation of flumequine and oxytetracycline antibiotics under visible light irradiation. J Mater Sci 55:4005–4016. https://doi.org/10.1007/s10853-019-04299-6

[4] Zhao R, Sun X, Jin Y, Han J, Wang L, Liu F (2019) Au/Pd/g-C_3N_4 nanocomposites for photocatalytic degradation of tetracycline hydrochloride. J Mater Sci 54:5445–5456. https://doi.org/10.1007/s10853-018-03278-7

[5] Zhang H, Liu P, Feng Y, Yang F (2013) Fate of antibiotics during wastewater treatment and antibiotic distribution in the effluent-receiving waters of the yellow Sea. Northern China. Mar Pollut Bull 73:282–290

[6] Du J, Zhao H, Liu S, Xie H, Wang Y, Chen J (2017) Antibiotics in the coastal water of the South Yellow Sea in China: occurrence, distribution and ecological risks. Sci Total Environ 595:521–527

[7] Ao X, Liu W (2017) Degradation of sulfamethoxazole by medium pressure UV and oxidants: peroxymonosulfate, persulfate, and hydrogen peroxide. Chem Eng J 313:629–637

[8] Yang Y, Lu X, Jiang J et al (2017) Degradation of sulfamethoxazole by UV, UV/H_2O_2 and UV/persulfate (PDS): formation of oxidation products and effect of bicarbonate. Water Res 118:196–207

[9] Zhu W, Sun F, Goei R, Zhou Y (2017) Facile fabrication of RGO-WO_3 composites for effective visible light photocatalytic degradation of sulfamethoxazole. Appl Catal B-Environ 207:93–102

[10] Ye P, Wu D, Wang M, Wei Y, Xu A, Li X (2018) Coating magnetic $CuFe_2O_4$ nanoparticles with OMS-2 for enhanced degradation of organic pollutants via peroxymonosulfate activation. Appl Surf Sci 428:131–139

[11] Tan C, Dong Y, Fu D, Gao N, Ma J, Liu X (2018) Chloramphenicol removal by zero valent iron activated peroxymonosulfate system: Kinetics and mechanism of radical generation. Chem Eng J 334:1006–1015

[12] Xing M, Xu W, Dong C, Bai Y, Zeng J, Zhou Y, Zhang J, Yin Y (2018) Metal sulfides as excellent Co-catalysts for H_2O_2 decomposition in advanced oxidation processes. Chem 4:1359–1372

[13] Yao Y, Lu F, Zhu Y, Wei F, Liu X, Lian C, Wang S (2015) Magnetic core–shell $CuFe_2O_4@C_3N_4$ hybrids for visible light photocatalysis of Orange II. J Hazard Mater 297:224–233

[14] Zhang C, Ou Y, Lei W-X, Wan L-S, Ji J, Xu Z-K (2016) $CuSO_4$/H_2O_2-induced rapid deposition of polydopamine coatings with high uniformity and enhanced stability. Angew Chem 128:3106–3109

[15] Naim S, Ghauch A (2016) Ranitidine abatement in chemically activated persulfate systems: Assessment of industrial iron waste for sustainable applications. Chem Eng J 288:276–288

[16] Qi C, Liu X, Ma J, Lin C, Li X, Zhang H (2016) Activation of peroxymonosulfate by base: implications for the degradation of organic pollutants. Chemosphere 151:280–288

[17] Tsitonaki A, Petri B, Crimi M, MosbÆK H, Siegrist RL, Bjerg PL (2010) In situ chemical oxidation of contaminated soil and groundwater using persulfate: a review. Crit Rev Env Sci Technol 40:55–91

[18] Anipsitakis GP, Dionysiou DD (2004) Radical generation by the interaction of transition metals with common oxidants. Environ Sci Technol 38:3705–3712

[19] Ball DL, Edwards JO (1956) The kinetics and mechanism of the decomposition of caro's acid I. J Am Chem Soc 78:1125–1129

[20] Ji Y, Fan Y, Liu K, Kong D, Lu J (2015) Thermo activated persulfate oxidation of antibiotic sulfamethoxazole and structurally related compounds. Water Res 87:1–9

[21] Matzek LW, Carter KE (2016) Activated persulfate for organic chemical degradation: a review. Chemosphere 151:178–188

[22] Li X, Yu J, Li G et al (2018) TiO2 nanodots anchored on nitrogen-doped carbon nanotubes encapsulated cobalt nanoparticles as photocatalysts with photo-enhanced catalytic activity towards the pollutant removal. J Colloid Interface Sci 526:158–166

[23] Lin K-YA, Lai H-K, Tong S (2018) One-step prepared cobalt-based nanosheet as an efficient heterogeneous catalyst for activating peroxymonosulfate to degrade caffeine in water. J Colloid Interface Sci 514:272–280

[24] Zeng H, Zhang W, Deng L et al (2018) Degradation of dyes by peroxymonosulfate activated by ternary CoFeNi-layered double hydroxide: catalytic performance, mechanism and kinetic modeling. J Colloid Interface Sci 515:92–100

[25] Chen F, Cao Y, Jia D (2013) A facile route for the synthesis of ZnS rods with excellent photocatalytic activity. Chem Eng J 234:223–231

[26] De Luca A, Dantas RF, Esplugas S (2014) Assessment of iron chelates efficiency for photo-Fenton at neutral pH. Water Res 61:232–242

[27] Rajabi HR, Khani O, Shamsipur M, Vatanpour V (2013) High-performance pure and Fe^{3+} ion doped ZnS quantum dots as green nanophotocatalysts for the removal of malachite green under UV-light irradiation. J Hazard Mater 250–251:370–378

[28] Yang Q, Choi H, Chen Y, Dionysiou DD (2008) Heterogeneous activation of peroxymonosulfate by supported cobalt catalysts for the degradation of 2,4-dichlorophenol in water: The effect of support, cobalt precursor, and UV radiation. Appl Catal B-Environ 77:300–307

[29] Hu Y, Chen K, Li Y-L et al (2019) Morphology-tunable WMoO nanowire catalysts for the extremely efficient elimination of tetracycline: kinetics, mechanisms and intermediates. Nanoscale 11:1047–1057

[30] Anipsitakis GP, Dionysiou DD (2003) Degradation of organic contaminants in water with sulfate radicals generated by the conjunction of peroxymonosulfate with cobalt. Environ Sci Technol 37:4790–4797

[31] Lu LT, Dung NT, Tung LD, Thanh CT, Quy OK, Chuc NV, Maenosono S, Thanh NTK (2015) Synthesis of magnetic cobalt ferrite nanoparticles with controlled morphology, monodispersity and composition: the influence of solvent, surfactant, reductant and synthetic conditions. Nanoscale 7:19596–19610

[32] Shen J, Lu Y, Liu J-K, Yang X-H (2016) Design and preparation of easily recycled $Ag_2WO_4@ZnO@Fe_3O_4$ ternary nanocomposites and their highly efficient degradation of antibiotics. J Mater Sci 51:7793–7802. https://doi.org/10.1007/s10853-016-0063-9

[33] Wu K, Qin Z, Zhang X, Guo R, Ren X, Pu X (2020) Z-scheme $BiOCl/Bi–Bi_2O_3$ heterojunction with oxygen vacancy for excellent degradation performance of antibiotics and dyes. J Mater Sci 55:4017–4029. https://doi.org/10.1007/s10853-019-04300-2

[34] Duan X, Su C, Miao J, Zhong Y, Shao Z, Wang S, Sun H (2018) Insights into perovskite-catalyzed peroxymonosulfate activation: Maneuverable cobalt sites for promoted evolution of sulfate radicals. Appl Catal B-Environ 220:626–634

[35] Yao Y, Cai Y, Wu G, Wei F, Li X, Chen H, Wang S (2015) Sulfate radicals induced from peroxymonosulfate by cobalt manganese oxides ($Co_xMn_{3−x}O_4$) for Fenton-Like reaction in water. J Hazard Mater 296:128–137

[36] Zhang T, Zhu H, Croué J-P (2013) Production of sulfate radical from peroxymonosulfate induced by a magnetically separable $CuFe_2O_4$ spinel in water: efficiency, stability, and mechanism. Environ Sci Technol 47:2784–2791

[37] Sun B, Guan X, Fang J, Tratnyek PG (2015) Activation of manganese oxidants with bisulfite for enhanced oxidation of organic contaminants: the Involvement of Mn(III). Environ Sci Technol 49:12414–12421

[38] Sundar M, Easwaramoorthy D, Kutti Rani S, Mohammed Bilal I (2008) Mn(II) catalysed decomposition of peroxomonosulphate—kinetic and mechanistic study. Catal Commun 9:2340–2344

[39] Xu W-H, Wang L, Wang J, Sheng G-P, Liu J-H, Yu H-Q, Huang X-J (2013) Superparamagnetic mesoporous ferrite nanocrystal clusters for efficient removal of arsenite from water. CrystEngComm 15:7895–7903

[40] Li Y, He J, Zhang K et al (2019) Super rapid removal of copper, cadmium and lead ions from water by NTA-silica gel. RSC Adv 9:397–407

[41] Al-Anazi A, Abdelraheem WH, Han C et al (2018) Cobalt ferrite nanoparticles with controlled composition-peroxymonosulfate mediated degradation of 2-phenylbenzimidazole-5-sulfonic acid. Appl Catal B-Environ 221:266–279

[42] Zhang S, Zhao X, Niu H, Shi Y, Cai Y, Jiang G (2009) Superparamagnetic Fe_3O_4 nanoparticles as catalysts for the catalytic oxidation of phenolic and aniline compounds. J Hazard Mater 167:560–566

[43] Wang B, Sun J, Abbas M, Liu Y, Kong F, Xiao H, Chen J (2017) A Novel hydrothermal approach for the synthesis of flower-Like Fe_2O_3/Fe foam Nanocrystals and their superior performance in fisher-tropsch synthesis. Catal Lett 147:1153–1161

[44] Zhu H, Yang D, Zhu L, Yang H, Jin D, Yao K (2007) A facile two-step hydrothermal route for the synthesis of γ-Fe_2O_3 nanocrystals and their magnetic properties. J Mater Sci 42:9205–9209. https://doi.org/10.1007/s10853-007-1887-0

[45] Fu Y, Chen Q, He M, Wan Y, Sun X, Xia H, Wang X (2012) Copper ferrite-graphene hybrid: a multifunctional heteroarchitecture for photocatalysis and energy storage. Ind Eng Chem Res 51:11700–11709

[46] Wang Z, Ma H, Zhang C, Feng J, Pu S, Ren Y, Wang Y (2018) Enhanced catalytic ozonation treatment of dibutyl phthalate enabled by porous magnetic Ag-doped ferrospinel $MnFe_2O_4$ materials: Performance and mechanism. Chem Eng J 354:42–52

[47] Descostes M, Mercier F, Thromat N, Beaucaire C, Gautier-Soyer M (2000) Use of XPS in the determination of chemical environment and oxidation state of iron and sulfur samples: constitution of a data basis in binding energies for Fe and S reference compounds and applications to the

evidence of surface species of an oxidized pyrite in a carbonate medium. Appl Surf Sci 165:288–302

[48] Zhou Y, Xiao B, Liu S-Q et al (2016) Photo-Fenton degradation of ammonia via a manganese–iron double-active component catalyst of graphene–manganese ferrite under visible light. Chem Eng J 283:266–275

[49] Wang G, Zhao D, Kou F, Ouyang Q, Chen J, Fang Z (2018) Removal of norfloxacin by surface Fenton system ($MnFe_2O_4/H_2O_2$): Kinetics, mechanism and degradation pathway. Chem Eng J 351:747–755

[50] Tan C, Gao N, Fu D, Deng J, Deng L (2017) Efficient degradation of paracetamol with nanoscaled magnetic $CoFe_2O_4$ and $MnFe_2O_4$ as a heterogeneous catalyst of peroxymonosulfate. Sep Purif Technol 175:47–57

[51] Su Y, Jiang H, Zhu Y, Yang X, Shen J, Zou W, Chen J, Li C (2014) Enriched graphitic N-doped carbon-supported Fe_3O_4 nanoparticles as efficient electrocatalysts for oxygen reduction reaction. J Mater Chem A 2:7281–7287

[52] Guan Y-H, Ma J, Ren Y-M, Liu Y-L, Xiao J-Y, Lin L-q, Zhang C (2013) Efficient degradation of atrazine by magnetic porous copper ferrite catalyzed peroxymonosulfate oxidation via the formation of hydroxyl and sulfate radicals. Water Res 47:5431–5438

[53] Li L, Abe Y, Kanagawa K, Usui N, Imai K, Mashino T, Mochizuki M, Miyata N (2004) Distinguishing the 5,5-dimethyl-1-pyrroline N-oxide (DMPO)-OH radical quenching effect from the hydroxyl radical scavenging effect in the ESR spin-trapping method. Anal Chim Acta 512:121–124

[54] Zhou Y, Wang X, Zhu C, Dionysiou DD, Zhao G, Fang G, Zhou D (2018) New insight into the mechanism of peroxymonosulfate activation by sulfur-containing minerals: role of sulfur conversion in sulfate radical generation. Water Res 142:208–216

[55] Moan J, Wold E (1979) Detection of singlet oxygen production by ESR. Nature 279:450–451

[56] Nohara K, Hidaka H, Pelizzetti E, Serpone N (1996) Dependence on chemical structure of the production of NH4+and/or NO3−3ions during the photocatalyzed oxidation of nitrogen-containing substances at the titania/water interface. Catal Lett 36:115–118

[57] Deng Y, Mao Y, Li B, Yang C, Zhang T (2016) Aerobic degradation of sulfadiazine by arthrobacter spp: kinetics, pathways, and genomic characterization. Environ Sci Technol 50:9566–9575

[58] Liu Y, Fan Q, Wang J (2018) Zn-Fe-CNTs catalytic in situ generation of H_2O_2 for Fenton-like degradation of sulfamethoxazole. J Hazard Mater 342:166–176